

ACOUSTIC MATCH OF A FREE-PISTON STIRLING ENGINE AND A LINEAR ALTERNATOR BASED ON THERMOACOUSTIC THEORY

Jie Zhang^{1,2}, Daming Sun^{1,2*}, Yun Qi^{1,2}, Honghao Pan^{1,2}

1 Institute of Refrigeration and Cryogenics, Zhejiang University, Hangzhou 310027, PR China

2 Key Laboratory of Refrigeration and Cryogenic Technology of Zhejiang Province, Hangzhou 310027, PR China

ABSTRACT

Stirling engines, especially free-piston Stirling engines (FPSE), have drawn more attention with the advantages of high thermal efficiency, constant power output, the flexibility to use any heat source as input and low noise. Acoustic impedance match is critical to the overall performances of a free-piston Stirling generator (FPSG). Based on thermoacoustic theory, the acoustic impedance characteristics of the FPSE and the linear alternator are calculated and analyzed individually. And the acoustic impedance of the FPSE and the linear alternator are then well matched. In the calculation, the FPSG output the electric power of 6223.2 W with the thermal-to-electric efficiency of 38.3% at the heating temperature of 900 K. The acoustic match approach would be helpful for designing FPSGs.

Keywords: Stirling, impedance, acoustic match, engine, linear alternator

NONMENCLATURE

<i>Abbreviations</i>			
FPSE	Free-piston Stirling engine	FPSG	Free-piston Stirling generator
HHX	Hot heat exchanger	REG	Regenerator
AHX	Ambient heat exchanger		
<i>Symbols</i>			
Z_{AHX}	Impedance at end of CHX	Z_{Eng}, Z_{Alt}	Impedance of engine/alternator
P_1, U_1	Amplitude of pressure and volume flow rate	P_m	Mean pressure
α, β	Phase difference between pressure and volume flow rate at the end of AHX/ power piston	ω	Angular frequency
γ	Specific heat ratio	k	magnetic spring constant

L_e	inductance of alternator	C_e	Electrical capacitance
X_e, X_m	Electrical/mechanical reactance	$R_{mech,d}$	Mechanical resistance of displacer/ power piston
R_e	Electric resistance of load and coil	$R_{mech,p}$	
Re, Im	Real/ imaginary part	Bl	Force factor
A	Area of power piston facing the engine	V	Volume of compression space
		i	$i = \sqrt{-1}$

1. INTRODUCTION

Due to the limit of fossil fuel resources and the requirements for environmental protection, the Stirling cycle mechanical devices have become a research hotspot today. Stirling engines have many advantages such as high thermal efficiency, constant power output, the flexibility to use any heat source as input and very less noise [1]. And the invention of FPSEs removed the technical barrier by replacing the rotary motor with a linear one [2]. The innovative configuration eliminates the drawbacks of the kinematic Stirling engine and leads to high reliability and zero maintenance [3]. Thus, FPSE and FPSG can be utilized in the area of combined heat and power (CHP) systems, solar energy generation, and space exploration, etc.

In 1990s, MTI developed opposed FPSGs system named SP-100 whose output electric power achieved 25 kW and thermal-to-electric efficiency reached 20% [4]. Sunpower Corporation also designed and produced 12 kW FPSG which received heat from fluid NaK of 850 K [5,6]. Besides, in 2000, Sunpower Corporation successfully developed a domestic micro-CHP system based on a FPSG referred to as EG-1000 [7]. This system can produce a net output electric power of 1 kW with an overall thermal efficiency of 90%. And Infinia Corporation also developed 1 kWe and 3kWe FPSGs for micro-CHP systems and solar dish-Stirling systems [8].

Actually, there are close analogies between the FPSE and thermoacoustic engine in terms of acoustic resonance and acoustic field tuning [3]. A FPSE can be regarded as a special thermoacoustic system from the perspective of thermoacoustics. Therefore, a FPSE can be designed and optimized through thermoacoustic theory. Yang et al. first used thermoacoustic theory to analyze the thermodynamic performance of a modified FPSE with a thermal buffer tube [9]. And Zhu et al. analyzed the acoustic impedance of a FPSG for a micro-CHP system based on thermoacoustic theory [3].

We have designed a traveling-wave thermoacoustic engine through the acoustic match approach [10], which was confirmed by the experiment. Thus, in this paper, the acoustic impedance match in a FPSG is studied numerically. And the general procedure to match the FPSE and the linear alternator to reach acoustical resonance is presented.

2. PROCEDURE OF ACOUSTIC MATCH

2.1 Model of FPSG

A schematic diagram of a 6 kWe FPSG, which is a β -type FPSE acoustically coupled with a linear alternator, is shown in Fig. 1. The FPSE mainly comprises a HHX, a REG, an AHX, and a displacer. The alternator mainly consists of a power piston and an electromagnetic circuit.

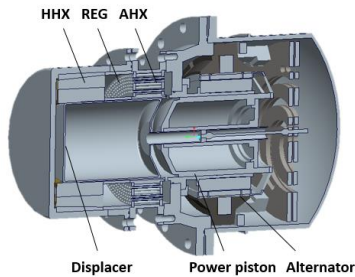


Fig 1 Schematic diagram of the 6 kWe FPSG

Firstly, to design the 6 kWe FPSE, Sage developed by Gedeon Associates was used in the study for the fundamental thermodynamic and dynamic calculations. Secondly, Ansys Maxwell was obtained to design the linear alternator. Thirdly, the FPSE and linear alternator are designed to resonate through the acoustic impedance match approach.

The main design geometry parameters are given in Table. 1. The working gas is helium of 3.5 MPa, the working frequency is 60 Hz, the heating temperature is 900 K, and the cooling temperature is 300 K.

Table 1 Main components and parameters of FPSG

Component	Details
-----------	---------

HHX	Fins, length 90 mm, channel width 0.6 mm, height 34.5 mm, number of fins 150
REG	length 55 mm, inner diameter 127mm, outer diameter 210 mm, filled with stainless steel fiber with a wire diameter of 21 μ m and a porosity of 91%
AHX	Shell-and-tube type, length 60 mm, tube inner diameter 2.6 mm, outer diameter 3.6 mm, number of tubes 570
Expansion space	Diameter 127 mm, roughly 400cc
Compression space	Diameter 127 mm, rod diameter 20 mm, roughly 250cc
Displacer	Diameter 127 mm facing the hot side, rod diameter 20 mm, moving mass 1.68 kg, spring constant 239 kN/m, nominal mechanical resistance around 30 N·s/m, amplitude 12 mm, phase between displacer and power piston 60°
Power piston	Diameter 127 mm, moving mass 2.3 kg, nominal mechanical resistance around 10 N·s/m, amplitude 16mm
Linear alternator	Motor constant 148 N/A, magnetic spring stiffness 139 kN/m, number of conductor 250, magnet mass 3.09 kg

2.2 Acoustic match theory

A FPSE can be simplified to the form of the engine shown in Fig 2 from the perspective of thermoacoustics. And the coupling interface is the surface of the power piston facing the FPSE.

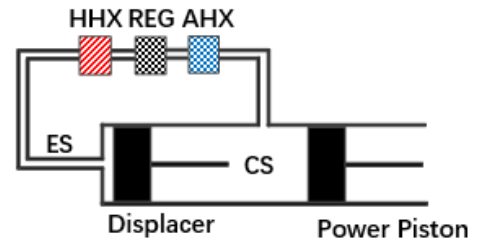


Fig 2 The FPSE from the perspective of thermoacoustics

2.2.1 Output acoustic impedance of the FPSE

Based on the model developed by Sage, the impedance at the end of the AHX can be calculated:

$$Z_{AHX} = \frac{P_1}{U_1} \quad (1)$$

The compression space is regarded as pure acoustic compliance. Thus, the pressure wave amplitude is constant for the inertance of the compression space is zero. And the volume flow rate difference between the end of the AHX and the coupling interface is:

$$\Delta U_1 = -\frac{i\omega V}{\gamma P_m} P_1 \quad (2)$$

Therefore, the output acoustic impedance of the FPSE is:

$$Z_{Eng} = \frac{P_1}{U_1 + \Delta U_1} \quad (3)$$

2.2.2 Input acoustic impedance of the linear alternator

The acoustic impedance of a linear alternator is expressed as follows [11]:

$$Z_{Alt} = \frac{1}{A^2} \left[\left(R_{mech,p} + \frac{R_e (Bl)^2}{R_e^2 + X_e^2} \right) + i \left(X_m - \frac{X_e (Bl)^2}{R_e^2 + X_e^2} \right) \right] \quad (4)$$

$$X_m = \omega M - k / \omega \quad (5)$$

$$X_e = \omega L_e - 1 / \omega C_e \quad (6)$$

2.2.3 Impedance match

From the perspective of thermoacoustics, a FPSG is a kind of acoustic resonance system that works by matching the acoustic impedances of the FPSE and linear alternator. The impedance match principle is displayed as follows:

$$Z_{Eng} = Z_{Alt} \quad (7)$$

$$\text{Re}(Z_{Eng}) = \text{Re}(Z_{Alt}) \quad (8)$$

$$\text{Im}(Z_{Eng}) = \text{Im}(Z_{Alt}) \quad (9)$$

It is worth noting that Equation 8 accounts for the displacement of the power piston and Equation 9 shows the basic principle for obtaining the resonant frequency [3]. The resonant frequencies for the FPSE and linear alternator should be the same or close. Thus, the working frequencies for the FPSE and alternator are both 60 Hz in the design.

2.3 Results and discussion

2.3.1 Output acoustic impedance of the FPSE

Fig 3 shows the numerical results about the pressure wave and volume flow rate at the end of the AHX. From Fig 3, the phase difference between the pressure and volume flow rate is 72° . Based on Equation 2, the volume flow rate difference ΔU_1 is $-i0.00953 \text{ m}^3/\text{s}$. And the phasor diagram of pressure and volume flow rate for the compression space is shown in Fig 4. So the phase difference β is 61.4° . And the acoustic impedance of the FPSE is $Z_{Eng} = 5.66 \times 10^6 + i1.04 \times 10^7 \text{ Pa} \cdot \text{s} / \text{m}^3$.

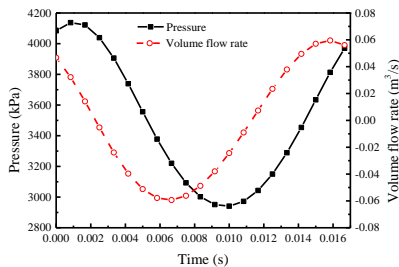


Fig 3 Pressure wave and volume flow rate at the end of AHX

Based on thermoacoustic theory, the larger the real part of the acoustic impedance, the higher the output

acoustic power, and the closer the angle approaches 90° , the lower the thermal efficiency [3].

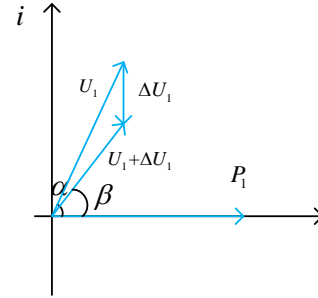


Fig 4 Phasor diagram for the compression space

2.3.2 Input acoustic impedance of the alternator

As seen from Equation 4, electrical inductance, capacitance and resistance, which are easy to adjust, have great impact on the impedance of the alternator. In this paper, the electrical inductance is set at 100 mH, and the influence of the electrical capacitance and resistance on the impedance is studied.

The acoustic impedance of the alternator varies with the resistance of the load and coil is displayed in Fig 5 and Fig 6. Based on Equations 7-9, when the electrical capacitance is about $100 \mu\text{F}$, and the resistance is about 25.0Ω , the output acoustic impedance of the FPSE is close to the input acoustic impedance of the alternator. Therefore, by adjusting the electrical capacitance, resistance and inductance, the acoustic impedance of the FPSE and the alternator can be well matched.

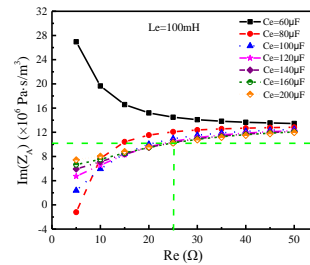


Fig 5 Imaginary part of the acoustic impedance of the alternator

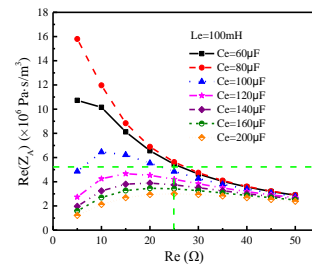


Fig 6 Real part of the acoustic impedance of the alternator

2.3.3 Performance of the FPSG

It is verified that the acoustic match between the FPSE and linear alternator can be achieved in the design. And based on Sage and Ansys Maxwell, the performance of the FPSG is obtained.

Fig 7 illustrates the PV power and the efficiency of the FPSE at different heating temperatures. Higher the heating temperature, larger the PV power and higher the efficiency. And with the increase of the heating temperature, the PV power increases faster and the efficiency increases more slowly. The PV power is 7585 W and the efficiency is 46.68% when the heating temperature is 900 K.

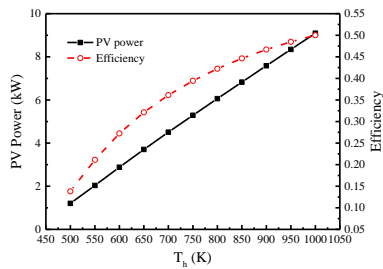


Fig 7 PV power and efficiency of the FPSE at different heating temperature

Fig 8 displays the output electric power of the linear alternator. As can be seen, the output electric power is 6223.2 W, when the displacement is 16mm, AC voltage is 640 V and AC current is 12.5 A. Moreover, when the heating temperature is 900 K, the PV power provided by the FPSE is large enough to be converted to the electric power and the thermal-to-electric efficiency is 38.3%.

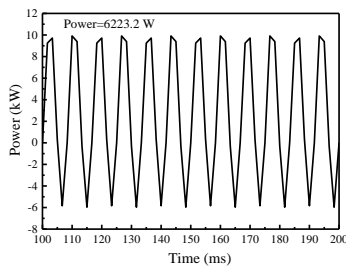


Fig 8 Output electric power of the linear alternator

2.4 Conclusions

The impedance match of a FPSE and a linear alternator is studied based on thermoacoustic theory. The general procedure for the impedance match is proposed systematically. Firstly, the acoustic impedance characteristics of the FPSE and the linear alternator are calculated and analyzed separately. Secondly, the acoustic impedance of the FPSE and the linear alternator

are well matched by adjusting the electrical inductance, capacitance and resistance. In our design, the numerical output electric power of the FPSG is 6223.2 W with the thermal-to-electric efficiency of 38.3% at the mean pressure of 3.5 MPa and the heating temperature of 900 K.

ACKNOWLEDGEMENT

This work is financially supported by National Key Research and Development Program (2016YFB0901403) and National Natural Science Foundation of China (NO. 51676168).

REFERENCE

- [1]Babaelahi M, Sayyaadi H. A new thermal model based on polytropic numerical simulation of Stirling engines. Appl. Energy 2015;141:143–159
- [2]Walker G, Senft JR. Free piston Stirling engines. Berlin, Heidelberg: SpringerVerlag; 1985
- [3]Zhu S, Yu G, O J, et al. Modeling and experimental investigation of a free-piston Stirling engine-based micro-combined heat and power system. Appl. Energy 2018;226:522-533
- [4]Schreiber JG. Assessment of the free-piston Stirling convertor as a long life power convertor for space. Energy Conversion Engineering Conference and Exhibit, 2000. (IECEC) 35th Intersociety. IEEE, 2000;2:1239-1247
- [5]Wood JG, Buffalino A, Holliday E. Free-piston Stirling power conversion unit for fission surface power, phase I final report. NASA/CR-2010-216750.
- [6]Wood JG, Stanley J. Free-piston Stirling power conversion unit for fission surface power, phase II final report. NASA/CR-2016-219088.
- [7]Kim SY, Huth J, Wood JG. Performance characterization of Sunpower free piston Stirling engines. In: 3rd International Energy Conversion Engineering Conference: San Fransisco, California;2005
- [8]<https://www.qnergy.com/smart-boiler/>
- [9]Yang Q, Luo E, Dai W, et al. Thermoacoustic model of a modified free piston Stirling engine with a thermal buffer tube. Appl. Energy 2012;90(1):266-270
- [10]Wang K, Zhang J, Zhang N, et al. Acoustic matching of a traveling-wave thermoacoustic electric generator. Appl. Therm. Eng. 2016;102:272-282
- [11]Sun D, Wang K, Zhang X, et al. A traveling-wave thermoacoustic electric generator with a variable electric R-C load. Appl. Energy 2013;106:377-382